AIP ADVANCES **5**, 067168 (2015)

Uncertainty analysis for the coefficient of band-to-band absorption of crystalline silicon

Carsten Schinke,[1,a] P. Christian Peest,[1] Jan Schmidt,[1,2] Rolf Brendel,[1,2]
Karsten Bothe,[1] Malte R. Vogt,[2] Ingo Kröger,[3] Stefan Winter,[3]
Alfred Schirmacher,[3] Siew Lim,[4] Hieu T. Nguyen,[4] and Daniel MacDonald[4]
[1]*Institute for Solar Energy Research Hamelin (ISFH), Am Ohrberg 1, 31860 Emmerthal, Germany*
[2]*Leibniz University of Hanover (LUH), Institute for Solid State Physics, Appelstraße 2, 30167 Hannover, Germany*
[3]*Physikalisch-Technische Bundesanstalt (PTB), Bundesallee 100, 38116 Braunschweig, Germany*
[4]*The Australian National University (ANU), College of Engineering and Computer Science, Canberra, ACT 0200, Australia*

(Received 18 March 2015; accepted 19 June 2015; published online 29 June 2015)

We analyze the uncertainty of the coefficient of band-to-band absorption of crystalline silicon. For this purpose, we determine the absorption coefficient at room temperature (295 K) in the wavelength range from 250 to 1450 nm using four different measurement methods. The data presented in this work derive from spectroscopic ellipsometry, measurements of reflectance and transmittance, spectrally resolved luminescence measurements and spectral responsivity measurements. A systematic measurement uncertainty analysis based on the *Guide to the expression of uncertainty in measurement* (GUM) as well as an extensive characterization of the measurement setups are carried out for all methods. We determine relative uncertainties of the absorption coefficient of 0.4% at 250 nm, 11% at 600 nm, 1.4% at 1000 nm, 12% at 1200 nm and 180% at 1450 nm. The data are consolidated by intercomparison of results obtained at different institutions and using different measurement approaches. [http://dx.doi.org/10.1063/1.4923379]

I. INTRODUCTION

Crystalline silicon is an important semiconductor material for a wide variety of applications, ranging from microelectronics and generation of electricity with solar cells to sensors for imaging methods or fundamental physical research. Many of these applications make use of the absorption or transmission of light within silicon and require a precise knowledge of the absorption coefficient. The determination of the absorption coefficient of crystalline silicon is thus an ongoing subject of research since 1955.[1–36] However, almost all of the published studies investigate the absorption coefficient only in a part of the wavelength range being of interest for a specific application. Moreover, different measurement methods were used. A comparison of literature data shows deviations of up to ±30% between the different data sets, as visualized in Fig. 1. It is unclear whether the deviations are only due to the specific properties of the investigated samples or whether they originate from systematic deviations or uncertainties due to the different measurement approaches. The accuracy of the literature data cannot be assessed since measurement uncertainties have not been determined systematically or, as for the major part of the studies, have not been indicated at all. This lack of information casts doubt on the accuracy of combined data sets which have been calculated from different sources. Moreover, only incomplete information about the properties of the samples

[a]Electronic mail: c.schinke@isfh.de

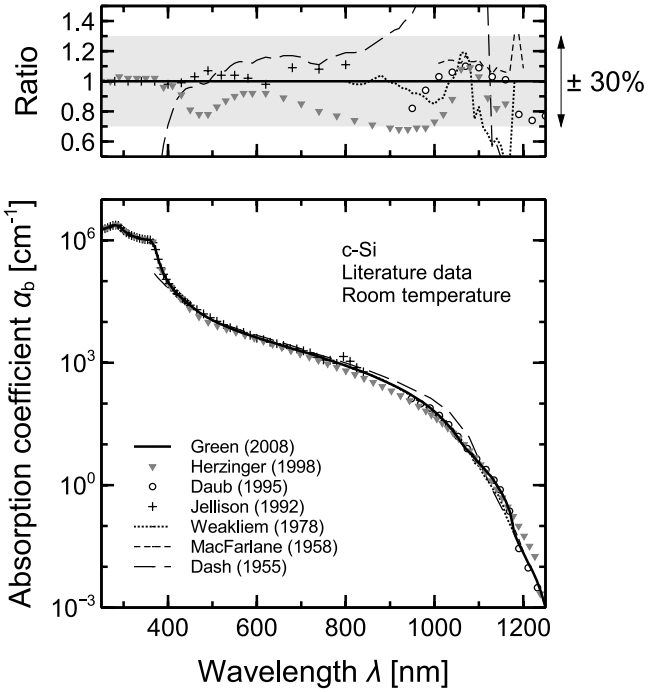

FIG. 1. Comparison of the most widely used data of the coefficient of band-to-band absorption of crystalline silicon α_{bb}. The top graph shows the ratio of the data compared to the most recent data by Green.[32]

as well as measurement conditions such as sample temperature, doping concentration, thickness or surface roughness is found in most of the studies. Unfortunately, for the older works the data are not available in tabulated form. Digitizing the data adds an additional uncertainty of unknown extent.

This paper aims at resolving the discrepancies found in the literature. For this purpose, measurements of the coefficient of band-to-band absorption of crystalline silicon are carried out using spectroscopic ellipsometry, measurements of reflectance and transmittance, spectrally resolved measurements of luminescence emission and measurements of the spectral responsivity of silicon solar cells. Together, these methods cover the wavelength range from 250 to 1450 nm. The measurements are carried out under well defined laboratory conditions. For each method, a systematic measurement uncertainty analysis is carried out. The analysis is based on an extensive characterization of the measurement setups and follows the *Guide to the expression of uncertainty in measurement* (GUM).[37] The resulting absorption coefficient data are consolidated by intercomparison of measurement results obtained at different institutions and using different measurement methods. In order to ensure usability of the results, tabulated data are given in this paper and also provided in digital form.

The paper starts with a brief review of the theoretical background of the applied measurement approaches. Afterwards, the measurement setups and samples are described and the measurement uncertainty analysis is outlined. The fourth part of the paper discusses the need of corrections for free carrier absorption and the calculation of a combined data set from the results of the different measurements.

II. METHODOLOGY

A. Definition of the absorption coefficient

Absorption of light in crystalline silicon is isotropic. The fundamental absorption process in the ultraviolet, visible and near-infrared spectral range (wavelengths below 1100 nm) is the inter-band absorption where electrons from the valence band are excited into the conduction band. For photon

energies above 3.4 eV, direct transitions are possible.[7] For lower photon energies, indirect transitions occur by the absorption or emission of phonons. In the following, this process will be referred to as *band-to-band absorption*. Photons may also be absorbed by either intra-band or band-impurity absorption. Intra-band absorption is caused by the excitation of an electron within the conduction band into a state of higher energy within the same band. This absorption process (also known as *free carrier absorption*, FCA) is often termed *parasitic absorption* as it does not generate additional free charge carriers but may hamper the functionality of electronic devices such as solar cells or photodiodes. Band-impurity absorption denotes the excitation of an electron within the conduction band into a state within the band gap which is induced by an impurity. The transition can occur from the impurity state to the conduction band as well. Band-impurity absorption occurs at low photon energies and does not interfere with band-to-band absorption. It is therefore not considered further in this paper.

The absorption coefficient α is defined by the relation

$$-\frac{d^2}{dz^2}\,\Phi(\lambda, z) = \alpha(\lambda)\,\Phi(\lambda, z)\,, \tag{1}$$

where the z-axis points in the direction of the photon flux Φ and λ is the photon wavelength. It contains both band-to-band and free carrier absorption, i.e.,

$$\alpha = \alpha_{\mathrm{bb}} + \alpha_{\mathrm{fc}}\,. \tag{2}$$

The solution of Eq. (1) is the common Lambert-Beer absorption law,

$$\Phi(\lambda, z) = \Phi_0(\lambda)\,\exp\big(-\alpha(\lambda)z\big)\,, \tag{3}$$

where Φ_0 denotes the initial photon flux density.

B. Principle of measurements

1. Spectroscopic ellipsometry

Ellipsometric measurements determine the change in the degree of polarization of light that undergoes a reflection at a surface. Specifically, a change Δ in phase difference between the parallel and perpendicular components of the incoming and outgoing light wave is measured, as well as a parameter Ψ which relates to the ratio of the reflection coefficients for the parallel and perpendicular components of the light wave. The spectroscopic ellipsometer used in this work measures both Ψ and Δ as a function of wavelength λ and the angle of incidence γ. The complex index of refraction is obtained from the measured polarization data by fitting with a suitable optical model for the layer stack. The fit is carried out separately for each wavelength. The extinction coefficient $\kappa(\lambda)$, which forms the imaginary part of the complex index of refraction, is related to the absorption coefficient by

$$\alpha(\lambda) = \frac{4\pi\kappa(\lambda)}{\lambda}\,. \tag{4}$$

In order to obtain smooth, Kramers-Kronig consistent data curves, a dispersion relation can be fitted to the discrete values of Ψ and Δ obtained for each wavelength. The fit can be extended to longer wavelengths by also taking transmittance data into account. This fit curve is referred to as *function fit* in the following and represents the dielectric function. Further details on ellipsometric measurements are found in the standard literature, e.g., Ref. 38. The method is applicable in the wavelength range where the extinction coefficient is large enough to be measured. For silicon, this corresponds to wavelengths below approximately 950 nm.

2. Reflectance / Transmittance measurements

For a planar sample (plan-parallel slab), reflectance R, transmittance T and absorption coefficient α are related by

$$R = R_s \left(1 + \frac{(1 - R_s)^2 \exp(-2\alpha W)}{1 - R_s^2 \exp(-2\alpha W)}\right) \tag{5}$$

and

$$T = \frac{(1 - R_s)^2 \exp(-\alpha W)}{1 - R_s^2 \exp(-2\alpha W)} \,. \tag{6}$$

In the latter equations, R_s denotes the surface reflectance and W the thickness of the sample. The absorption coefficient is given by

$$\alpha = -\frac{1}{W} \ln\left(\frac{C - R^2 + 2R + T^2 - 1}{2T}\right), \tag{7}$$

where

$$C = \sqrt{(R^2 - 2R - T^2 - 1)^2 - 4(2 - R)R} \,. \tag{8}$$

Equations (5) through (8) follow from taking an infinite number of internal reflections into account, using the limit value of the infinite geometric series[39] and solving the system of equations for α. Note that these equations refer to perpendicular incidence of light. Using the relations for the experimental determination of the absorption coefficient requires to collect all reflected/transmitted light.

3. Spectrally resolved luminescence measurements

Luminescence emission originates from the radiative recombination of electrons and holes within the sample. The emitted luminescence photon flux per wavelength interval and surface area $\Phi(\lambda)$ is given by[40–42]

$$\Phi(\lambda) = \int_0^W dz\, r_{ph}(\lambda, z) f_{esc}(\lambda, z) \,, \tag{9}$$

where f_{esc} is the luminescence photon escape probability and r_{ph} is the spectral photon generation rate per wavelength interval. r_{ph} is defined by the generalized Planck radiation law for luminescence[43] and depends on the absorption coefficient α. It can be shown[31] that under typical luminescence measurement conditions, Eq. (9) can be approximated by

$$\Phi(\lambda) \approx \alpha_{bb}(\lambda) \frac{8\pi\, c\, n_{Si}^2(\lambda)}{\lambda^4} \times \int_0^W dz\, f_{esc}(\lambda, z) \exp\left(\frac{\mu_{ph}(z) - \frac{hc}{\lambda}}{kT}\right), \tag{10}$$

where c is the speed of light, n_{Si} is the refractive index of silicon, μ_{ph} is the chemical potential of the photons (given by the splitting of the quasi-Fermi levels), h is the Planck constant, k is the Boltzmann constant, T is the sample temperature and f_{esc} is the luminescence photon escape probability. The latter equation shows that the coefficient of band-to-band absorption is proportional to the luminescence spectrum. In two special cases, the relation between the absorption coefficient and the luminescence spectrum simplifies:[23] a) If the charge carrier concentration within the sample is homogenous, μ_{ph} is independent of z and the luminescence spectrum becomes proportional to the absorptance of the sample. b) If the absorption coefficient is small, f_{esc} is independent of z and the luminescence spectrum becomes proportional to the absorption coefficient. For wafer samples as used in this work, the second approximation holds for wavelengths above 1200 nm. In both cases, only relative luminescence intensities need to be measured. However, the determination of the scaling factor requires previously determined absolute values of the absorptance or absorption coefficient, respectively.

4. Spectral responsivity measurements

The spectral responsivity $SR(\lambda)$ of a photodiode or solar cell at wavelength λ is defined as short circuit current per incident intensity of light. From the spectral responsivity, the external quantum

efficiency EQE is calculated via

$$EQE(\lambda) = SR(\lambda)\,\frac{hc}{q\lambda} \tag{11}$$

where q is the elementary charge. By an optical reciprocity theorem optical reciprocity theorem,[44] the EQE and consequently the SR are connected to the electroluminescence photon flux Φ_{EL} of the device by[42]

$$\Phi_{\mathrm{EL}}(\lambda,\Omega)d\lambda d\Omega = \Phi_{\mathrm{bb}}(\lambda,\Omega)d\lambda d\Omega\, EQE(\lambda,\Omega)\, \exp\left(\frac{V}{V_{\mathrm{T}}}\right), \tag{12}$$

where Ω is the solid angle into which the photons are emitted, V is the junction voltage, $V_{\mathrm{T}} = kT/q$ is the thermal voltage and

$$\Phi_{\mathrm{bb}}(\lambda,\Omega)\, d\lambda d\Omega = \frac{2c}{\lambda^4}\, \exp\left(-\frac{hc}{\lambda kT}\right)\, d\lambda d\Omega\,. \tag{13}$$

Electroluminescence spectrum and SR can thus be transformed vice versa and the same theory as for the determination of the absorption coefficient from luminescence spectra (see section II B 3) applies to SR data.

C. Systematic uncertainty analysis

The measurement uncertainty analysis carried out in this work is based on the *Guide to the Expression of Uncertainty in Measurement*[37] (GUM). The GUM is the international standard for the systematic evaluation of measurement uncertainties. This section briefly summarizes the terminology and methodology used in this publication. For a definition of metrological terminology, the reader is referred to Ref. 45.

In many experiments, a measurand Y is not measured directly but calculated from other quantities X_i whose values are determined in the experiment. The *process equation* describes the functional relationship

$$Y = f(X_1,\ldots,X_{\mathrm{N}})\,. \tag{14}$$

between the *input quantities* X_{i} and the *output quantity* Y. The values of the quantities are denoted by the corresponding lowercase letters, i.e., y and x_i. The uncertainty of a measured value is given by its probability distribution function, as visualized in Fig. 2. Recurrent probability distribution functions are the normal (gaussian) distribution, the rectangular distribution and the triangular distribution. These distributions are visualized in Fig. 2.

The *combined standard uncertainty* $u_c(y)$ of the output quantity is the positive square root of the combined variance of the output quantity. The *level of confidence* (also called *coverage probability*) for a given uncertainty indicates the probability that a measurement will yield a result which deviates from the expectation value of the measurement by not more than the specified uncertainty. The *expanded uncertainty* U for a desired level of confidence is obtained by multiplication of u with a *coverage factor* k:

$$U(y) = k\, u_{\mathrm{c}}(y)\,. \tag{15}$$

The value of k for a given level of confidence is determined by the distribution function of the quantity. For a normal distribution, the combined standard uncertainty corresponds to a confidence level of approximately 68 %. The expanded uncertainty for a $k = 2$, which is used throughout this publication, corresponds to a coverage probability of approximately 95 %.

The equality of two measurement results x_1 and x_2 with respect to their uncertainty is assessed quantitatively by calculating the E_{n}-number

$$E_{\mathrm{n}} = \frac{1}{k}\,\frac{|x_1 - x_2|}{\sqrt{u_c^2(x_1) + u_c^2(x_2)}}\,, \tag{16}$$

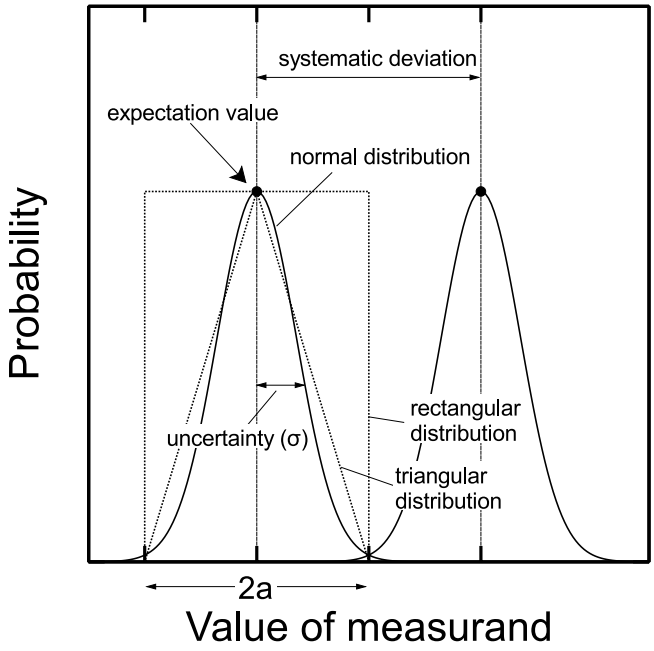

FIG. 2. Visualization of *uncertainty* and *systematic deviation* in a measurement and recurrent probability distribution functions.

which is used in international key comparisons as a criterion for measurement compatibility.[46] In Eq. (16), k is the coverage factor defined above which must be equal for both measurements. In this publication, compatibility is accepted if

$$E_n \leq 1 \tag{17}$$

holds, which means that the difference between the two measurement results, $|x_1 - x_2|$, is smaller than the expanded uncertainty of this difference for $k = 2$, $\sqrt{(2\,u_c(x_1))^2 + (2\,u_c(x_2))^2}$.

III. MEASURING THE ABSORPTION COEFFICIENT

The measurements presented in this publication are carried out at ISFH as well as the PTB. Figure 3 shows an overview of the measurements with respect to wavelength and method. The following paragraphs provide information about the samples, the measurement setups and the data evaluation procedures.

A. Spectroscopic ellipsometry

Spectroscopic ellipsometry is carried out in the wavelength range from 250 to 930 nm on a front side chemo-mechanically polished monocrystalline Czochralski grown p-type silicon wafer sample with a resistivity of 5 Ωcm and a thickness of 1284 µm. The rear surface is optically rough. After polishing, the sample is RCA cleaned. The sample temperature is (295 ± 1) K. The measurements are carried out with a commercially available M-2000 UI (rotating compensator) ellipsometer manufactured by J. A. Woolam Co., Inc. This instrument is equipped with two detectors (Si and InGaAs) and allows for measurements within the wavelength range from 240 to 1700 nm. The sample is illuminated with white light from a halogen lamp, which is spectrally decomposed after interaction with the sample by a diffraction grating. The instrument is calibrated with respect to wavelength and polarization using the standard procedure recommended by the manufacturer. The acquisition and evaluation of the measured data is performed using the software WVASE32[47] provided by the manufacturer. The evaluation procedure consists of fitting the measured data (Ψ and

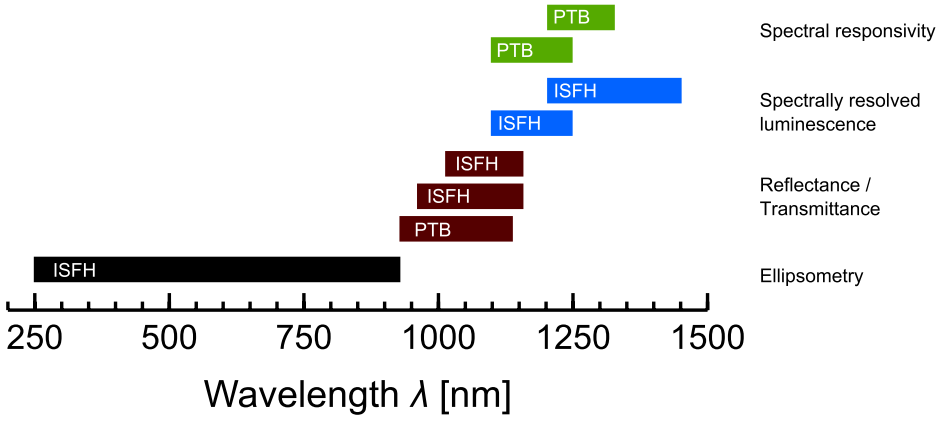

FIG. 3. Overview of measurements carried out in this work.

Δ) with an optical model of the layer stack. This fit is performed separately for each wavelength. Figure 4 shows the measured data (Ψ and Δ, represented by the markers) and the model fit (visualized by the corresponding lines) for the different angles of incidence γ (60°, 65°, 70°, 75°and 80°). The optical model used for the evaluation of the data assumes a planar silicon slab of thickness W which is covered by a thin layer of silicon oxide of thickness W_{SiO_2} (which is of the order of a few nm). The oxide layer is assumed since the samples are handled in air and the formation of an oxide layer cannot be prevented.[48] The optical constants of SiO_2 are retrieved from the optical constants database included in WVASE32. These data are denoted as *Thermal* SiO_2 *optical constants (Herzinger, 2008)* and are similar to, but not identical with, data published by Herzinger *et al.* in 1998.[30] The oxide thickness is determined from a fit of the data at wavelengths between 1200 and 1400 nm, where the absorptance of the silicon bulk is approximatly zero. The model further assumes that no light is reflected at the rear surface of the sample (which is equal to the assumption that only light which is reflected at the front surface of the sample is collected by the detector). This assumption is justified within the wavelength range analyzed by ellipsometric measurements.

The evaluation of the absorption coefficient from measured data of Ψ and Δ involves a fitting procedure. Therefore, uncertainties of Ψ and Δ cannot simply be propagated into the uncertainty of the absorption coefficient by using the analytical approach described in section II C. A *Monte-Carlo simulation* (MC simulation) as described in the GUM [Ref. 37, supplement 1] is a numerical approach for solving this task. Basically, it consists of many recalculations of the output quantity. On each iteration, all input quantities are randomly varied according to their probability distribution and a specific value of the output quantity is obtained. By calculation of the average and standard deviation of the output quantity, its value and uncertainty are determined. The Monte-Carlo approach has the advantage that it does not require an analytical process equation, which is not available in case of fitting algorithms.

The uncertainty analysis includes the following contributions: Uncertainties determined from repeated measurements of Ψ and Δ, uncertainty due to the optical properties of SiO_2, wavelength accuracy, spectral bandwidth, angle of incidence, alignment of optical components, nonlinearities of the detector or depolarization of light by the sample and reproducibility. The software WVASE32 is not capable of conducting such an analysis. The Monte-Carlo simulation is thus realized by generating the simulated (randomly varied) input data Ψ_{exp} and Δ_{exp} in Excel, loading the data into WVASE32, executing the fit procedure in WVASE32 and exporting the resulting n and κ data to Excel again, where the standard deviations for n and κ are finally calculated. This procedure is quite slow. For this reason, the simulation is terminated after 10000 iterations, which corresponds to about five days of calculation time on a standard desktop computer.

The resulting data for the coefficient of band-to-band absorption and its uncertainty are shown in Fig. 5. The circles show the results of the Monte-Carlo simulation. The shaded area indicates the resulting absolute uncertainty of the data, the blue dotted line represents the relative uncertainty. The uncertainty of the absorption coefficient resulting from ellipsometry increases to about 100%

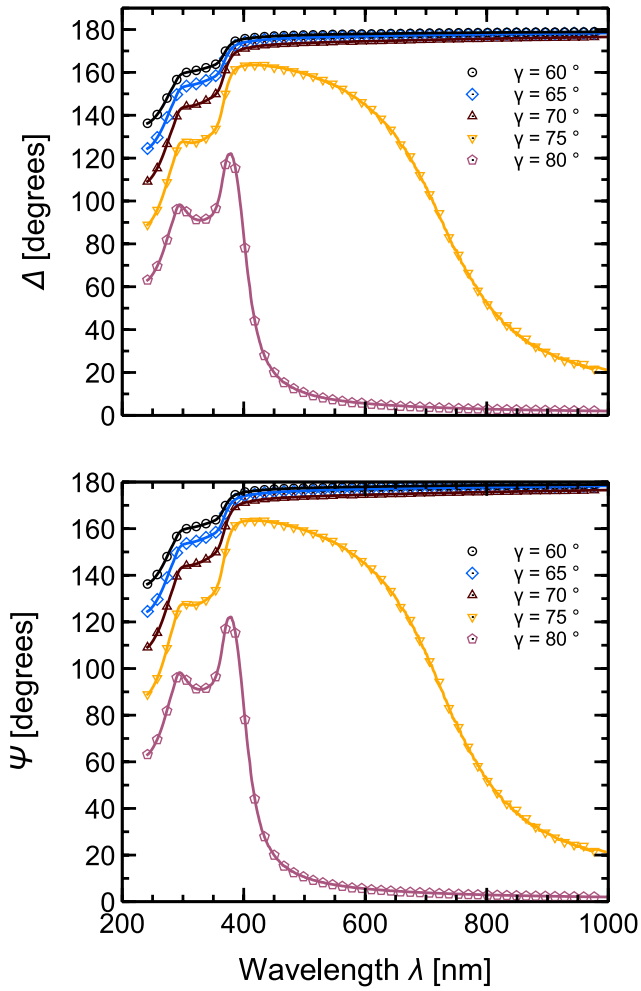

FIG. 4. Measured values $\Psi(\lambda, \gamma)$ and $\Delta(\lambda, \gamma)$ (markers) and model fit (corresponding lines). The different colors represent the different angles of incidence γ. For reasons of clarity, the number of data points shown in the figure is reduced.

rel. at 900 nm. The main reason for this is a decreasing signal-to-noise ratio, which results from the increasing ratio of real and imaginary part of the complex index of refraction. The dash-dotted line shows a function fit performed in WVASE32, which is extended into the infrared region by also taking transmittance data into account. The fit function consists of 5 Tauc-Lorentz oscillators and 2 gaussian shaped osciallators.[47,49] For comparison, the data obtained from RT measurements (see next section) is also shown. The function fit slightly deviates from the RT data around 930 nm. In order to obtain a better agreement with the accurate RT data, a Tauc parametrization[50] of the data using $\alpha = [\beta\,(hc/\lambda - E_G)]^2$ is performed in the wavelength range from 650 to 1050 nm and visualized by the solid red line. The expression is fitted to the data considering the uncertainty of the data as fit weights. The quantities β and E_G are free fit parameters, h represents the Planck constant and c is the speed of light. The uncertainty of the parametrization (red dotted line) is taken equal to the uncertainty of the data at 650 nm and 930 nm (the latter being given by the uncertainty of the RT data) and linearly interpolated inbetween. Hence, by combining ellipsometry and RT measurements, the uncertainty of the absorption coefficient above 650 nm is reduced.

B. Reflectance / Transmittance measurements

Reflectance/transmittance measurements are carried out on double side chemo-mechanically polished monocrystalline Czochralski grown p-type silicon wafers (supplied by Siltronic and

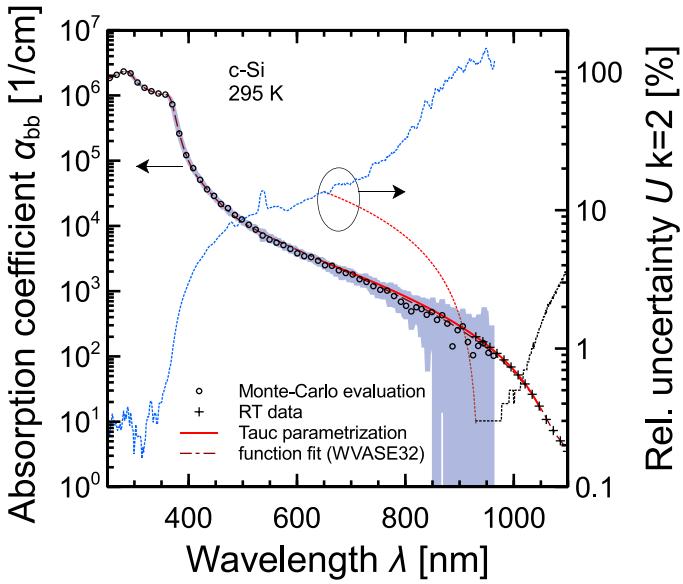

FIG. 5. Absorption coefficient α_{bb} and uncertainty obtained from spectroscopic ellipsometry. For comparison, the data resulting from RT measurements are also shown.

SunEdison) with an area of 3 × 3 cm^2 and a resistivity of 4 to 6 Ωcm. After polishing, the samples are RCA cleaned. The sample thickness is (653.0 ± 1.9) µm for sample RT-A and (1284.0 ± 1.5) µm for sample RT-B. The thickness is measured at four positions on the sample using a dial gauge. The sample temperature during the RT measurements is (295 ± 1) K. The measurements are performed with a commercially available Varian Cary 5000 two-channel spectrophotometer equipped with an integrating sphere accessory and a PbS detector. The system uses a halogen lamp in combination with a grating monochromator for the generation of monochromatic light. Behind the exit port of the monochromator, a chopper wheel reflects the light either into the sample channel or the monitor channel. The monitor channel is used to compensate for variations of the intensity of the monochromatic light over time and to adjust the detector pre-amplifier such that an optimal signal level is provided at the input of the A/D converter. A third position on the chopper wheel blocks the light. This position is used for the measurement of the internal dark signal of the detector.

The measurement uncertainty analysis considers repeatability of the measurements, nonlinearity of the detectors, spectral bandwidth, wavelength accuracy, tilt of the sample and angular incidence of light, scattering of light within the sample, uncertainty of the reference values (reflectance measurements) and long-term reproducibility. Moreover, a systematic deviation due to inertia of the detector / measurement amplifier is identified and corrected. The characterization of the measurement setup and the uncertainty analysis are described in detail in Ref. 51. The measured RT data are shown in Fig. 6. The solid lines represent the measured reflectance and transmittance, the corresponding dotted lines show the relative uncertainty of the data (k = 2). Figure 7 exemplary visualizes the uncertainty budget for the transmittance measurement using sample RT-B at 1050 and 1250 nm. The graph shows the relative contributions to the overall uncertainty of the measurand (each contribution is normalized to the overall uncertainty). It can be seen that in the wavelength range where the transmittance is not saturated, significant uncertainty contributions result from the spectral bandwidth of the monochromatic light, the accuracy of the wavelength calibration and measurement noise. However, decreasing the spectral bandwidth would result in an even lower signal-to-noise ratio and would thereby not decrease the overall uncertainty. However, the uncertainty of the data is generally small (≤ 1% rel. for most wavelengths).

Beside the measurements at ISFH, RT measurements are also carried out at PTB on samples from the same wafers. In these investigations, reflectance is determined by a combination of the results obtained with a VW-method in a commercial Varian Cary 6000i spectrophotometer as well as by applying a special setup with increased angle of acceptance in the primary national reference

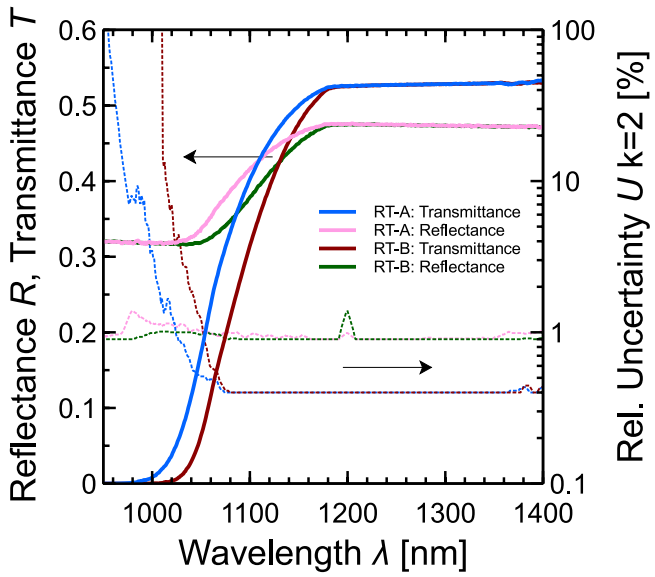

FIG. 6. Measured reflectance/transmittance data (solid lines) and rel. uncertainty of the data (dotted lines).

system for spectral reflectance. Figure 8 shows the absorption coefficient following from these measurements. All data are in agreement with respect to the uncertainty of the data. This is seen from the top graph, visualizing the E_n number. E_n is smaller than unity, which means that deviations between the data are explained by their uncertainty. Moreover, the figure shows that the uncertainty of the absorption coefficient determined from RT measurements increases strongly beyond

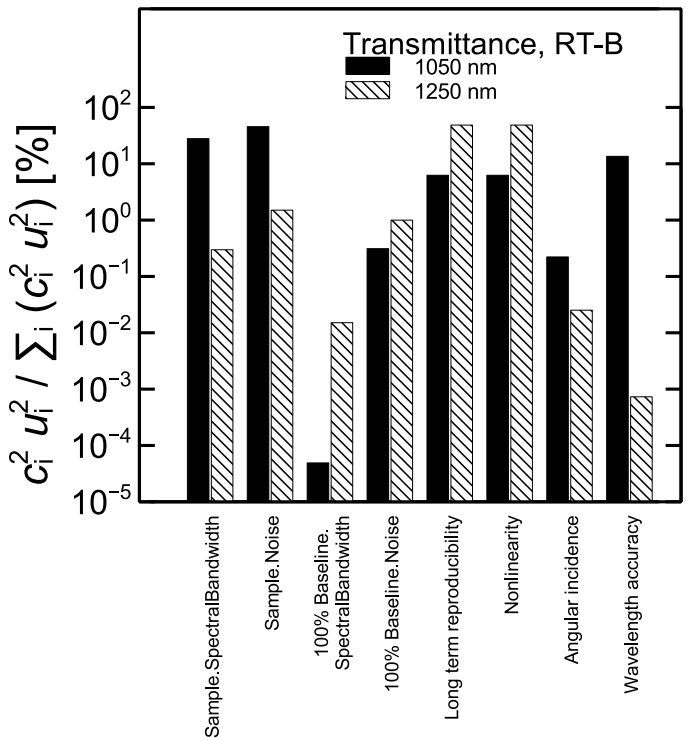

FIG. 7. Uncertainty budget for a transmittance measurement at 1050 and 1250 nm using sample RT-B. The graph shows the relative contributions to the overall uncertainty of the measurand.

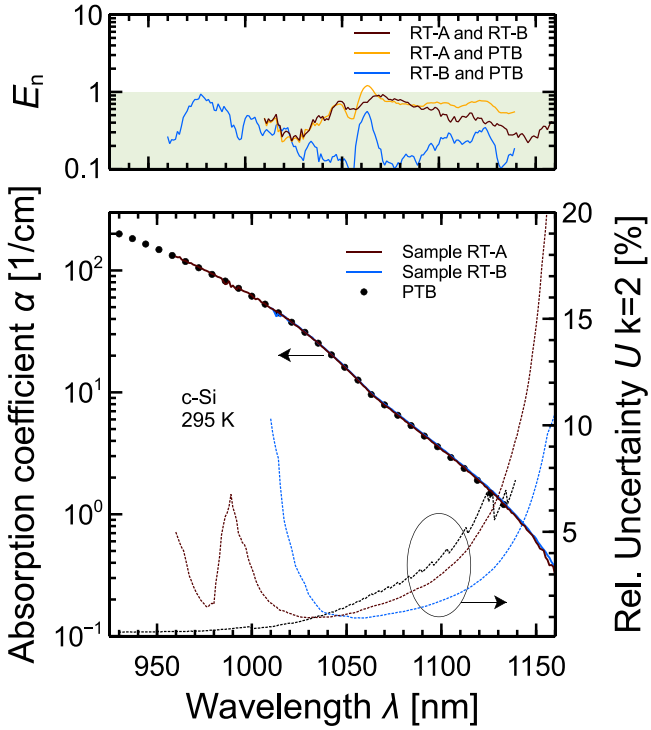

FIG. 8. Absorption coefficient α_{bb} of crystalline silicon at 295 K as determined from RT measurements (bottom) and E_n number for the data (top).

1150 nm. If RT data are used for the scaling of luminescence data as described in the next section, the scaling should thus be performed in the wavelength range below 1150 nm.

C. Spectrally resolved luminescence measurements

Spectrally resolved electroluminescence (EL) measurements are carried out in the wavelength range from 1100 to 1250 nm on specially designed lab-type solar cells with an area of 2×2 cm^2. These solar cells, made of *p*-type Czochralski grown silicon with a thickness of (711 ± 2) µm and a resistivity of 2.5 Ωcm, feature a chemo-mechanically polished front and rear surface. The surface metallization is achieved by evaporating a 10 µm thick layer of aluminium on the rear side and a grid structure (also 10 µm thick aluminium) on the front side. The solar cells do not have a back surface field nor an antireflection coating in order to preserve the polished surfaces. Additionally, a reference sample without front surface metallization is available, as well as a reference sample which is not metallized and where the emitter diffusion is applied to both sides of the sample. The reference samples are required for the experimental determination of surface reflectances and FCA in the emitter. Spectrally resolved photoluminescence (PL) measurements are carried out in the wavelength range from 1200 to 1450 nm on double side textured samples with an area of 3×3 cm^2 from the same wafers as for the RT measurements. The samples for PL are electrically passivated on both sides by 15 nm thick layers of atomic-layer-deposited Al_2O_3. The surface passivation increases the ratio of radiative and non-radiative recombination. The absorptance of the passivation layer is below 0.00001%, so that its presence does not affect the determination of the absorption coefficient. The sample temperature is (295 ± 0.5) K for all EL/PL measurements.

The measurements presented in this work are carried out using a commercially available scanning spectrometer system (InstrumentSystems Spectro 320 R5) which is equipped with a single monochromator and an InGaAs detector. The system is in-house calibrated in our ISO 17025 certified test center with respect to wavelength and irradiance against a mercury vapor lamp and a standard halogen lamp traceable to the PTB, respectively. The sample is placed on a temperature

controlled sample stage and its temperature is continuously monitored by a PT1000 temperature sensor attached to the front surface of the sample. The luminescence emission is collected perpendicular from above and transmitted into the spectrometer by a multi-core fiber cable equipped with a diffuser head. PL emission is excited by laser illumination from above. The laser emits light at a center wavelength of 808 nm. Underground illumination at other wavelengths is filtered out by an optical bandpass filter. The laser spot is widened by an array of micro lenses and homogeneously illuminates an area of 5×5 cm^2 with an intensity of about 70 mW/cm^2. The lateral irradiance variation is below 10 % rel. The sample stage is a black anodized brass plate with a reflectance of below 10 % within the wavelength range of interest. Raytracing simulations show that the presence of the brass plate does not affect the shape of the luminescence spectrum and thus does not affect the determination of the absorption coefficient. EL emission is excited by attaching a power supply and contacting the front busbar of the solar cell with Kelvin probes. The rear contact is made by the sample stage (a brass plate in case of EL measurements). Since the solar cells feature a rear surface metalization, the reflectance of the brass plate is irrelevant. The brass plate contains an additional PT1000 temperature sensor which is attached to the rear surface of the solar cell.

PL measurements on planar (double side polished) wafer samples show a dependence of the shape of the luminescence spectrum on the distance between the sample and the detector, as shown in Fig. 9. The top graph shows EL spectra of a planar solar cell (see section III), the bottom graph shows PL spectra of planar and textured wafers. All data are normalized to maximum. The dependence on the detection distance is not expected from theory and is not yet understood. It might eventually originate from luminescence emission from the edges of the sample. Another possibility is stray light from the excitation laser. This assumption is supported by the finding that the effect is neither observed for EL measurements nor for PL measurements on textured wafers, as shown in Fig. 9. Nevertheless, PL measurements on planar wafers introduce potential uncertainties for the determination of the absorption coefficient. For this reason, EL data are used from 1100 to 1250 nm. Above 1200 nm, PL data from a textured wafer are also taken into account. The wavelength range below 1100 nm is covered by RT data.

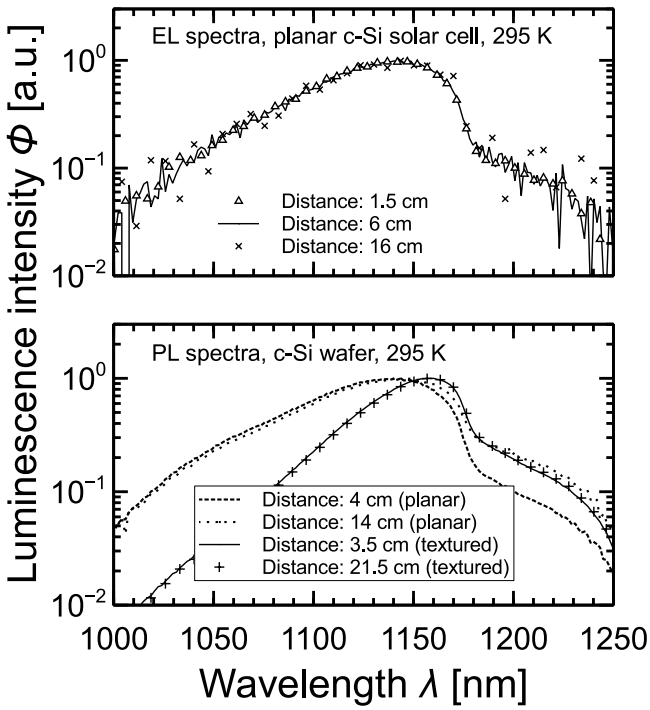

FIG. 9. EL/PL measurements with perpendicular detection at different distances between sample and detector. All data are normalized to maximum. The EL measurements feature a lower SNR than the PL measurements, especially at increased distances.

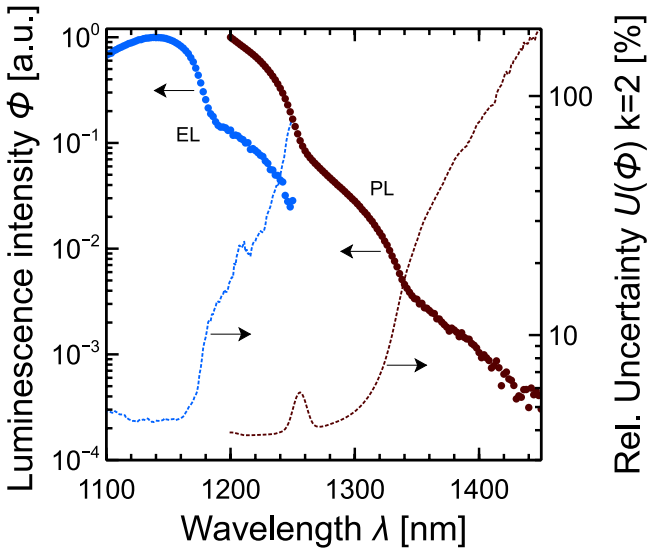

FIG. 10. Measured EL and PL spectra (markers) and relative uncertainty of the data (dotted lines). The measured data are normalized to maximum.

Figure 10 shows the measured EL and PL spectra (markers) and the relative uncertainty of the data (corresponding dotted lines). For comparison, the spectra are normalized to maximum. The uncertainty analysis for the luminescence measurements includes contributions due to repeatability of the measurements, spectral bandwidth, wavelength accuracy, drift of the detector's dark signal, nonlinearities of the detector regarding the irradiance, spectral stray light, long-term reproducibility and the uncertainty of the standard lamp calibration at the PTB. Figure 11 exemplary shows the uncertainty budget for the EL measurement on the planar solar cell at 1140 and 1200 nm. Since the planar solar cell features a fully metallized rear surface, the absorptance of the silicon bulk A_{Si} cannot be measured directly. Therefore, it is determined using RT measurements on a reference

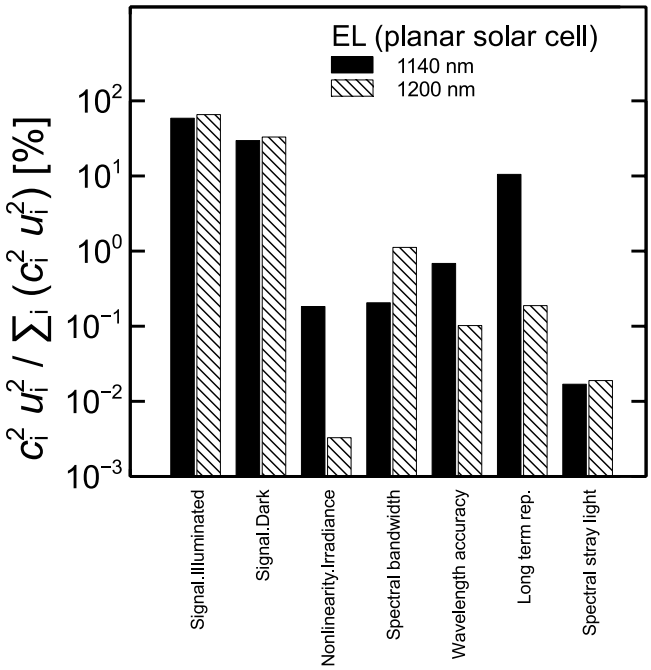

FIG. 11. Uncertainty budget for an exemplary EL measurement at 1140 and 1200 nm. The graph shows the relative contributions to the overall uncertainty of the measurand.

sample without surface metallization and the absorption coefficient data resulting from the RT measurements. The scaling factor C_{scale} for the EL data Φ is obtained as a weighted average over the data in the wavelength range from 1100 to 1140 nm, the weights being given by the uncertainty of the data:

$$C_{\mathrm{scale}} = \frac{\sum_{i=1}^{N} C_i/u^2(C_i)}{\sum_{i=1}^{N} 1/u^2(C_i)} \tag{18}$$

with

$$C_i = \frac{A_{\mathrm{Si}}(\lambda_{\mathrm{i}})}{\Phi(\lambda_{\mathrm{i}})} \tag{19}$$

and 1100 nm $\leq \lambda_{\mathrm{i}} \leq$ 1140 nm. The relative uncertainty of the C_{i} is of the order of 5%. Due to the small wavelength range used for scaling, the C_{i} are assumed to be fully correlated. According to the GUM, the uncertainty of C_{scale} then is

$$u^2(C_{\mathrm{scale}}) = \left(\frac{\sum_{i=1}^{N} 1/u(C_i)}{\sum_{i=1}^{N} 1/u^2(C_i)} \right)^2 . \tag{20}$$

The relative uncertainty $u(C_{\mathrm{scale}})$ of the scaling factor is 2.8%. The scaled luminescence data are obtained by multiplication with the scaling factor, $\Phi_{\mathrm{scaled}} = \Phi \times C_{\mathrm{scale}}$. From the scaled data, the absorption coefficient follows from the relation between the absorptance A of a planar sample and the absorption coefficient α,

$$A = (1 - R_{\mathrm{f}}) \frac{1 + (R_{\mathrm{b}} - 1)\exp(-\alpha W) - R_{\mathrm{b}}\exp(-2\alpha W)}{1 - R_{\mathrm{b}}R_{\mathrm{f}}\exp(-2\alpha W)} , \tag{21}$$

where R_{f} and R_{b} denote the reflectance of front and rear surface, respectively. The PL data are then scaled to the values of the absorption coefficient from EL in the wavelength range from 1200 to 1250 nm using the procedure described above for calculating the scaling factor. The scaling procedure is described in more detail in Ref. 52. The resulting absorption coefficient data are shown in Fig. 13 together with the results of the spectral responsivity measurements outlined in the next section.

D. Spectral responsivity measurements

For the measurements of spectral responsivity (SR), different samples are used. Industrial p-type silicon solar cells, cut down to an area of 2 × 2 cm^2, are used for SR measurements in the wavelength range from 1200 to 1320 nm. The polished lab solar cells described in the preceeding section are also used for SR measurements in the wavelength range from 1100 to 1250 nm. The sample temperature is (295 ± 0.5) K for all SR measurements. The measurements presented in this work are carried out at the PTB. The measurement setup and the uncertainty analysis are described in Refs. 53 and 54. Figure 12 shows the EQE following from these measurements. The circles represent the EQE data, the corresponding crosses indicate the relative uncertainty of the data. The dashed/dotted lines represent guides to the eye. The resulting absorption coefficient data are shown in Fig. 13 together with the results of the EL/PL measurements. The top graph shows the E_{n} number for the data. All data agree with respect to their uncertainty, which is reflected by $E_{\mathrm{n}} < 1$ for all wavelengths. This also provides experimental evidence for the underlying reciprocity theorem.[44]

IV. COMBINING THE DATA

It is desirable to combine the data presented in the preceding section into one set of data. The standard approach for combining different measurements of the same quantity is the calculation of a weighted average, the weights being given by the inverse squared uncertainty of the single measurement results. The uncertainty of the weighted average is usually calculated as the inverse sum of these weights, based on the assumption that the single results are uncorrelated. This assumption

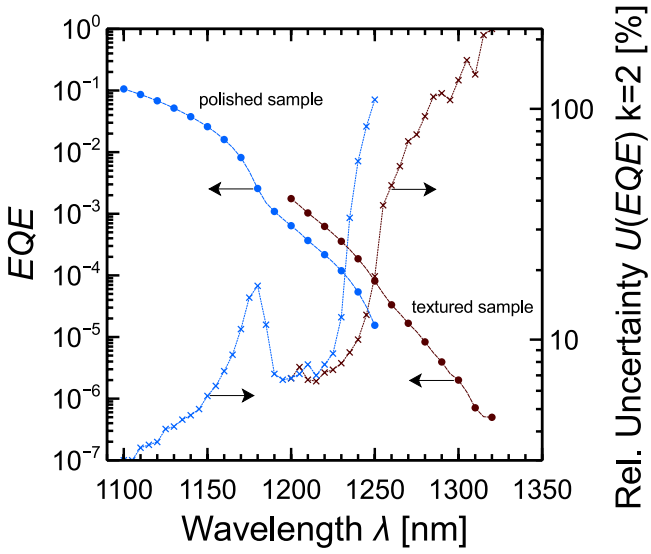

FIG. 12. Measured EQE data (circles) and relative uncertainty of the data (crosses). The dashed/dotted lines represent guides to the eye.

is questionable, for instance, if different data sets which are to be averaged are obtained using the same measurement setup, as is the case for the RT measurements carried out at ISFH. In case of correlations, the uncertainty of the weighted average would be underestimated. The uncertainty of the combined RT data is therefore calculated following the approach for the incorporation of hidden

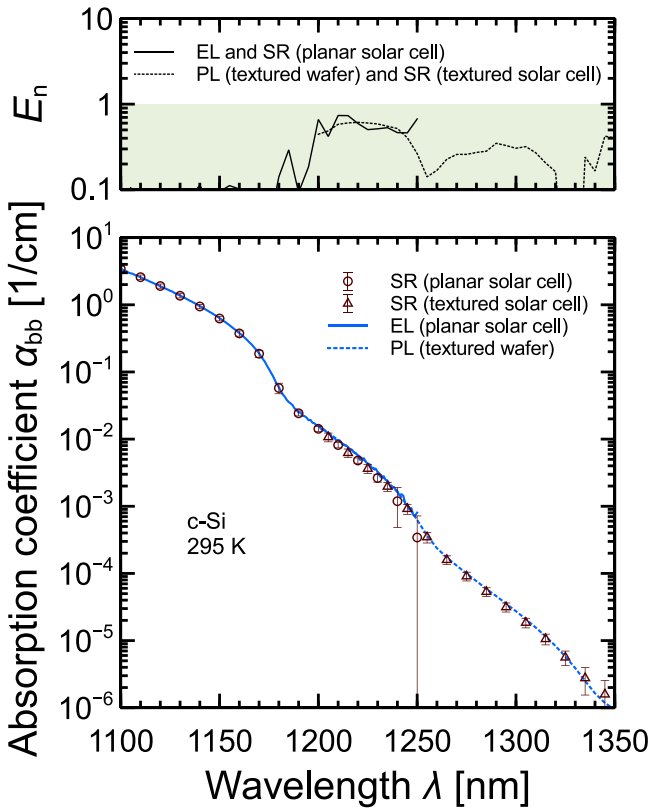

FIG. 13. Absorption coefficient α_{bb} of crystalline silicon at 295 K as determined from EL, PL and SR measurements (bottom) and E_n number for the data (top).

correlations into the calculation of a weighted average described in Ref. 55. Luminescence and spectral responsivity data are assumed to be uncorrelated, since different measurement methods and setups are used. For these data, the weighted average is calculated using the standard procedure mentioned above.

In order to obtain the coefficient of band-to-band absorption, corrections for free carrier absorption (FCA) must be considered. Ellipsometry data are available from measurements carried out at ISFH in the wavelength range from 250 to 930 nm. For the samples used in this work, the coefficient of free carrier absorption α_{fc} following from the FCA parametrization in Ref. 56 is below 10^{-2} cm^{-1} in this wavelength range, whereas the absorption coefficient is of the order of 10^2 to 10^6 cm^{-1}. Hence, $\alpha \approx \alpha_{bb}$ and corrections for FCA are not applied, since they are of the order of 0.0001 % rel. at most.

Measurements of reflectance and transmittance yield the absorption coefficient α, which contains contributions of both band-to-band absorption and free carrier absorption (FCA). The coefficient of band-to-band absorption is thus given by $\alpha_{bb} = \alpha - \alpha_{fc}$. In order to determine the coefficient of band-to-band absorption α_{bb}, the FCA parametrization from Ref. 56 is used for a doping concentration of 3×10^{15} cm^{-3}, which follows from the resistivity of the samples. The relative correction below 1150 nm, where data from RT measurements is used, is below 2 % and hardly visible on a logarithmic scale. As the accuracy of the FCA parametrization is unknown, the uncertainty of the correction is assumed to equal the correction itself and a rectangular distribution is assumed. The relative uncertainty of α_{bb} is thereby increased by about 0.2 % absolute at 1140 nm.

Luminescence and spectral responsivity measurements are carried out on various planar and textured samples. The measurands (photon flux or short circuit current) are affected by additional absorption due to free charge carriers. The incorporation of FCA into the evaluation of the data depends on the structure and doping concentration of the samples. For PL measurements on planar wafer samples, the impact of FCA is negligible due to the low doping concentration. The EL data requires a correction in the wavelength range below 1165 nm[52] due to FCA in the bulk of the solar cell. FCA in the emitter is taken into account by the experimentally determined rear surface reflectance of the solar cell, which is an effective reflectance and contains additional photon reabsorption due to FCA. Further corrections for FCA in the emitter are thus not necessary. Below 1140 nm, the correction for FCA in the bulk is equal to the correction for the RT data, to which the EL data are scaled. However, a doping concentration of 1.2×10^{16} cm^{-3}, which follows from the resistivity of the sample, is used for the calculation. Between 1140 and 1165 nm, the correction cannot be calculated rigorously and is therefore linearly interpolated. Again, the uncertainty of the correction is assumed to equal the correction itself and a rectangular distribution is assumed. The relative correction is below 4.5 % and hardly visible on a logarithmic scale. Due to these corrections, the relative uncertainty of α_{bb} is increased by about 1 % absolute at 1140 nm.

The SR data obtained from the industrial solar cell also requires a correction due to FCA in the emitter and back surface field of the solar cell. Here, FCA leads to a decrease of the short circuit current of the solar cell, which is the measurand. This leads to a variation of the (experimentally determined) scaling factor with respect to wavelength. The correction is calculated by using an analytical model for the charge carrier generation profile adapted from Ref. 57. Within the wavelength range where data from the industrial (textured) solar cell is available, the correction is of the order of not more than 6%, which is still hardly visible on a logarithmic scale. The correction does not change the relative uncertainty of the data by more than 0.01% absolute.

As a last step, the uncertainty of the absorption coefficient due to the uncertainty of the sample temperature during the measurements must be taken into account. For this purpose, the temperature coefficient

$$c_T(\lambda) = \frac{1}{\alpha_{bb}(\lambda, 295\ K)} \frac{d\alpha_{bb}(\lambda, T)}{dT}\Big|_{295\ K} \tag{22}$$

of the absorption coefficient is determined as an average of data following from spectroscopic ellipsometry carried out at ISFH, PL carried out at the ANU and data from Ref. 32, as shown in Fig. 14. The shaded area represents the standard deviation of the data. Tabulated data for Fig. 14 is given in the appendix (Table II). The uncertainty contribution due to uncertainty of the sample temperature is

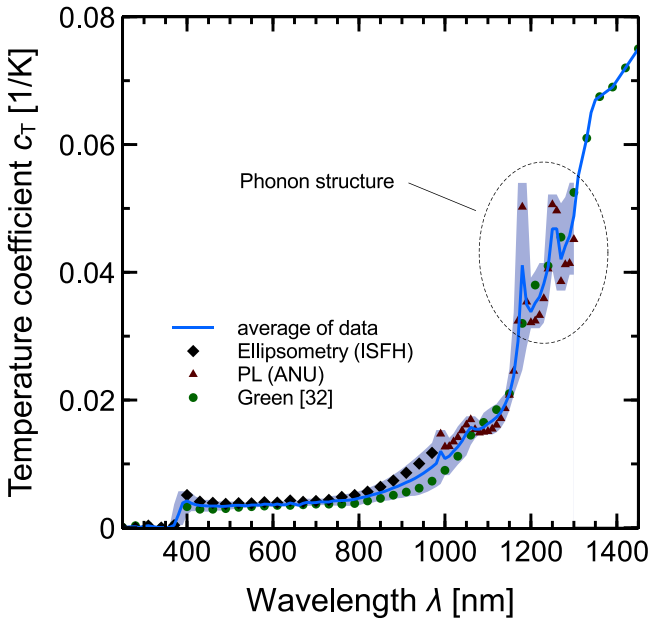

FIG. 14. Temperature dependence of the coefficient of band-to-band absorption, following from measurements carried out in this work, as well as from Refs. 32 and 35.

estimated by assuming a rectangularly distributed component of width $\alpha_{bb}\, c_T\, \Delta T$, where ΔT = 1 K for ellipsometry, reflectance and transmittance measurements and ΔT = 0.5 K for luminescence and spectral responsivity measurements, as indicated above. The overall relative uncertainty of the absorption coefficient is thereby increased by not more than 1% absolute.

The resulting data including the mentioned FCA corrections is shown in Fig. 15. Tabulated data are given in the appendix (Table I) and also available as supplemental electronic data for this publication.[58] Figure 16 compares the results to literature data. The bottom graph visualizes the absorption coefficient, the middle graph shows the ratio of the literature data to the data determined

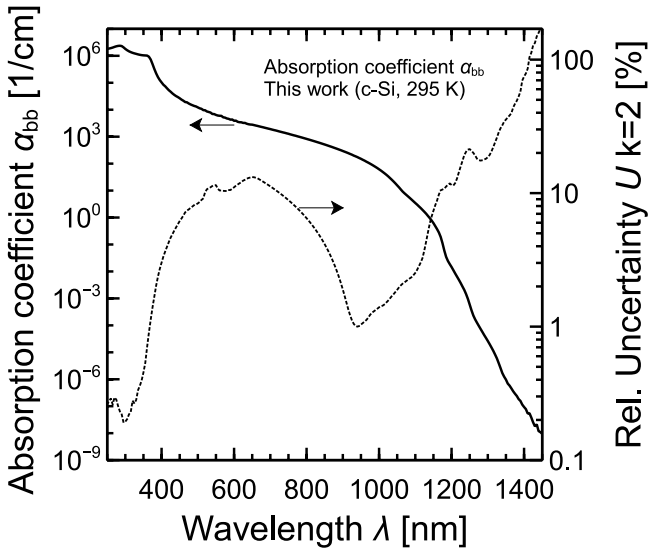

FIG. 15. Final data of the coefficient of band-to-band absorption of crystalline silicon at 295 K and its uncertainty as determined in this work. Tabulated data are given in the appendix (Table I) and also available as an electronic appendix for this publication.[58]

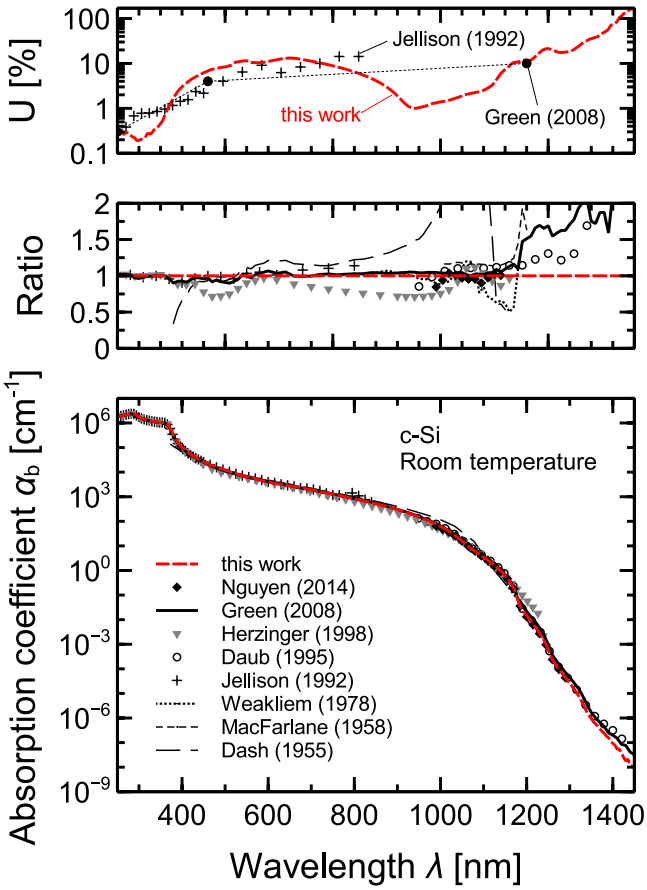

FIG. 16. Comparison of absorption coefficient data and its uncertainty as determined in this work and as found in the literature.

in this work. The top graph shows the uncertainty of the data (if available). For the data of Green, uncertainty estimates are only specified for three distinct wavelengths (visualized by the dots), the dotted line represents a guide to the eye. Regarding the values of the absorption coefficient, good agreement with the data by Green[32] is found, except for the wavelength range beyond 1200 nm. In this wavelength range, deviations between measured and expected luminescence spectra of silicon samples were reported when using the absorption coefficient data of Green as input for the model.[42,59] These deviations are resolved by the data obtained in this work.[60]

According to Ref. 32, the absorption coefficient can be transformed to other temperatures T using the relation

$$\alpha_{\mathrm{bb}}(T) = \alpha_{\mathrm{bb}}(T_0)\,(T/T_0)^b \tag{23}$$

where T_0 is the nominal temperature for the absorption coefficient data (295 K for the data in this paper) and

$$b = c_{\mathrm{T}}\,T_0 \tag{24}$$

incorporates the temperature coefficient.

V. CONCLUSION

The coefficient of band-to-band absorption of crystalline silicon at 295 K is determined under well defined laboratory conditions in the wavelength range from 250 to 1450 nm by means of spectroscopic ellipsometry, measurements of reflectance and transmittance, spectrally resolved

luminescence measurements and spectral responsivity measurements. A systematic measurement uncertainty analysis is carried out for each method, allowing to provide substantiated estimates for the uncertainty of the data. We determine relative uncertainties of 0.4% at 250 nm, 11% at 600 nm, 1.4% at 1000 nm, 12% at 1200 nm and 180% at 1450 nm. Data obtained at ISFH and PTB are compared and the agreement of the data with respect to their uncertainty is shown quantitatively. It is shown that the uncertainty of the absorption coefficient is mostly dominated by measurement noise resulting from a low signal-to-noise ratio. The latter is a consequence of the variation of the absorption coefficient over 13 orders of magnitude in the wavelength range analyzed. Moreover, it is shown that photoluminescence measurements on planar (polished) wafer samples introduce potential uncertainties for the determination of the absorption coefficient in the wavelength range from about 1100 to 1250 nm. For this reason, electroluminescence data are used in this wavelength range. The deviations to literature data are of the order of up to 30% relative and can only partly be explained by the uncertainty of the data determined in this work. This points towards systematic effects as the origin of the deviations.

ACKNOWLEDGMENT

The authors would like to thank Dr. E. Daub from Siltronic for his support and for providing polished silicon wafers. The support of Dr. B. Falster from Sun Edison, who provided polished silicon wafers, is also gratefully acknowledged. Many thanks also go to C. Marquardt and S. Mau from ISFH for processing the samples. Funding was provided by the scholarship program of the German Federal Environmental Foundation (Deutsche Bundesstiftung Umwelt) and the State of Lower Saxony. We acknowledge support by Deutsche Forschungsgemeinschaft and Open Access Publishing Fund of Leibniz Universität Hannover.

APPENDIX A: COEFFICIENT OF BAND-TO-BAND ABSORPTION OF CRYSTALLINE SILICON AT 295 K

TABLE I. Coefficient of band-to-band absorption of crystalline silicon at 295 K and its relative uncertainty as determined in this work. The uncertainty is specified for a coverage factor $k = 2$ and rounded to two significant digits.

λ [nm]	α_{bb} [cm^{-1}]	$\frac{U(\alpha_{bb})}{\alpha_{bb}}$ [%]	λ [nm]	α_{bb} [cm^{-1}]	$\frac{U(\alpha_{bb})}{\alpha_{bb}}$ [%]	λ [nm]	α_{bb} [cm^{-1}]	$\frac{U(\alpha_{bb})}{\alpha_{bb}}$ [%]
250	1.804×10^{6}	0.26	660	2.591×10^{3}	13	1070	7.965×10^{0}	2.2
260	1.930×10^{6}	0.28	670	2.402×10^{3}	13	1080	6.070×10^{0}	2.2
270	2.139×10^{6}	0.27	680	2.226×10^{3}	12	1090	4.585×10^{0}	2.3
280	2.332×10^{6}	0.28	690	2.061×10^{3}	12	1100	3.452×10^{0}	2.5
290	2.302×10^{6}	0.18	700	1.907×10^{3}	11	1110	2.594×10^{0}	2.8
300	1.797×10^{6}	0.19	710	1.763×10^{3}	11	1120	1.915×10^{0}	3.2
310	1.469×10^{6}	0.20	720	1.629×10^{3}	10	1130	1.377×10^{0}	4.1
320	1.289×10^{6}	0.25	730	1.503×10^{3}	9.8	1140	9.503×10^{-1}	5.8
330	1.178×10^{6}	0.32	740	1.386×10^{3}	9.3	1150	6.215×10^{-1}	7.8
340	1.093×10^{6}	0.30	750	1.276×10^{3}	8.9	1160	3.713×10^{-1}	8.8
350	1.044×10^{6}	0.43	760	1.173×10^{3}	8.4	1170	1.896×10^{-1}	10
360	1.017×10^{6}	0.66	770	1.078×10^{3}	7.9	1180	5.917×10^{-2}	11
370	7.269×10^{5}	1.1	780	9.882×10^{2}	7.4	1190	2.445×10^{-2}	12
380	3.254×10^{5}	1.7	790	9.049×10^{2}	7.0	1200	1.456×10^{-2}	11
390	1.621×10^{5}	2.4	800	8.271×10^{2}	6.5	1210	8.398×10^{-3}	12
400	1.025×10^{5}	3.0	810	7.546×10^{2}	6.0	1220	4.938×10^{-3}	13
410	7.395×10^{4}	3.7	820	6.871×10^{2}	5.5	1230	2.772×10^{-3}	17
420	5.294×10^{4}	4.3	830	6.243×10^{2}	5.1	1240	1.451×10^{-3}	22
430	4.023×10^{4}	5.0	840	5.659×10^{2}	4.6	1250	5.911×10^{-4}	22
440	3.199×10^{4}	5.5	850	5.116×10^{2}	4.1	1260	2.329×10^{-4}	20
450	2.663×10^{4}	6.1	860	4.612×10^{2}	3.7	1270	1.258×10^{-4}	18

Table I. (*Continued.*)

λ [nm]	α_{bb} [cm^{-1}]	$\frac{U(\alpha_{bb})}{\alpha_{bb}}$ [%]	λ [nm]	α_{bb} [cm^{-1}]	$\frac{U(\alpha_{bb})}{\alpha_{bb}}$ [%]	λ [nm]	α_{bb} [cm^{-1}]	$\frac{U(\alpha_{bb})}{\alpha_{bb}}$ [%]
460	2.161×10^{4}	6.8	870	4.145×10^{2}	3.2	1280	7.391×10^{-5}	17
470	1.878×10^{4}	7.5	880	3.713×10^{2}	2.8	1290	4.364×10^{-5}	18
480	1.566×10^{4}	7.8	890	3.313×10^{2}	2.3	1300	2.632×10^{-5}	18
490	1.380×10^{4}	8.0	900	2.945×10^{2}	1.9	1310	1.521×10^{-5}	20
500	1.220×10^{4}	8.3	910	2.605×10^{2}	1.5	1320	8.301×10^{-6}	24
510	1.080×10^{4}	8.9	920	2.293×10^{2}	1.2	1330	3.972×10^{-6}	28
520	9.553×10^{3}	9.3	930	1.994×10^{2}	1.0	1340	1.700×10^{-6}	33
530	8.252×10^{3}	11	940	1.746×10^{2}	0.98	1350	9.707×10^{-7}	36
540	6.957×10^{3}	12	950	1.507×10^{2}	1.0	1360	5.813×10^{-7}	38
550	6.406×10^{3}	11	960	1.286×10^{2}	1.1	1370	3.580×10^{-7}	42
560	5.958×10^{3}	11	970	1.089×10^{2}	1.2	1380	2.401×10^{-7}	50
570	5.235×10^{3}	10	980	9.147×10^{1}	1.3	1390	1.571×10^{-7}	58
580	4.744×10^{3}	10	990	7.570×10^{1}	1.4	1400	9.360×10^{-8}	75
590	4.276×10^{3}	11	1000	6.160×10^{1}	1.4	1410	5.385×10^{-8}	88
600	3.879×10^{3}	11	1010	4.929×10^{1}	1.4	1420	3.796×10^{-8}	120
610	3.555×10^{3}	12	1020	3.873×10^{1}	1.5	1430	1.791×10^{-8}	140
620	3.407×10^{3}	12	1030	2.934×10^{1}	1.6	1440	1.203×10^{-8}	170
630	3.245×10^{3}	13	1040	2.170×10^{1}	1.8	1450	9.447×10^{-9}	180
640	2.885×10^{3}	13	1050	1.561×10^{1}	1.9			
650	2.793×10^{3}	13	1060	1.096×10^{1}	2.0			

APPENDIX B: TEMPERATURE COEFFICIENT OF THE COEFFICIENT OF BAND-TO-BAND ABSORPTION OF CRYSTALLINE SILICON AT 295 K

TABLE II. Temperature coefficient c_T of α_{bb} at 295 K (Fig. 14).

λ [nm]	c_T [K^{-1}]	λ [nm]	c_T [K^{-1}]	λ [nm]	c_T [K^{-1}]	λ [nm]	c_T [K^{-1}]
250	4.500×10^{-5}	560	3.565×10^{-3}	870	5.969×10^{-3}	1180	4.111×10^{-2}
260	7.500×10^{-5}	570	3.555×10^{-3}	880	6.246×10^{-3}	1190	3.494×10^{-2}
270	1.550×10^{-4}	580	3.702×10^{-3}	890	6.486×10^{-3}	1200	3.382×10^{-2}
280	1.650×10^{-4}	590	3.674×10^{-3}	900	6.789×10^{-3}	1210	3.520×10^{-2}
290	4.000×10^{-5}	600	3.570×10^{-3}	910	7.104×10^{-3}	1220	3.614×10^{-2}
300	2.352×10^{-4}	610	3.719×10^{-3}	920	7.382×10^{-3}	1230	3.820×10^{-2}
310	3.261×10^{-4}	620	3.581×10^{-3}	930	7.723×10^{-3}	1240	4.077×10^{-2}
320	1.818×10^{-4}	630	3.617×10^{-3}	940	8.126×10^{-3}	1250	4.680×10^{-2}
330	8.743×10^{-5}	640	3.883×10^{-3}	950	8.543×10^{-3}	1260	4.682×10^{-2}
340	2.794×10^{-5}	650	3.711×10^{-3}	960	9.022×10^{-3}	1270	4.204×10^{-2}
350	$0.000\times10^{+0}$	660	3.513×10^{-3}	970	9.513×10^{-3}	1280	4.411×10^{-2}
360	7.000×10^{-5}	670	3.830×10^{-3}	980	1.007×10^{-2}	1290	4.570×10^{-2}
370	4.102×10^{-4}	680	3.992×10^{-3}	990	1.199×10^{-2}	1300	4.883×10^{-2}
380	2.054×10^{-3}	690	3.902×10^{-3}	1000	1.084×10^{-2}	1310	5.500×10^{-2}
390	3.894×10^{-3}	700	3.945×10^{-3}	1010	1.122×10^{-2}	1320	5.800×10^{-2}
400	4.208×10^{-3}	710	4.062×10^{-3}	1020	1.199×10^{-2}	1330	6.100×10^{-2}
410	3.843×10^{-3}	720	4.035×10^{-3}	1030	1.267×10^{-2}	1340	6.500×10^{-2}
420	3.612×10^{-3}	730	4.032×10^{-3}	1040	1.360×10^{-2}	1350	6.700×10^{-2}
430	3.494×10^{-3}	740	4.198×10^{-3}	1050	1.481×10^{-2}	1360	6.750×10^{-2}
440	3.450×10^{-3}	750	4.238×10^{-3}	1060	1.572×10^{-2}	1370	6.800×10^{-2}
450	3.405×10^{-3}	760	4.262×10^{-3}	1070	1.545×10^{-2}	1380	6.850×10^{-2}
460	3.402×10^{-3}	770	4.299×10^{-3}	1080	1.543×10^{-2}	1390	6.900×10^{-2}
470	3.411×10^{-3}	780	4.349×10^{-3}	1090	1.575×10^{-2}	1400	7.000×10^{-2}

Table II. (*Continued.*)

λ [nm]	c_T [K^{-1}]	λ [nm]	c_T [K^{-1}]	λ [nm]	c_T [K^{-1}]	λ [nm]	c_T [K^{-1}]
480	3.336×10^{-3}	790	4.461×10^{-3}	1100	1.630×10^{-2}	1410	7.100×10^{-2}
490	3.371×10^{-3}	800	4.636×10^{-3}	1110	1.674×10^{-2}	1420	7.200×10^{-2}
500	3.438×10^{-3}	810	4.774×10^{-3}	1120	1.730×10^{-2}	1430	7.300×10^{-2}
510	3.514×10^{-3}	820	4.925×10^{-3}	1130	1.806×10^{-2}	1440	7.400×10^{-2}
520	3.523×10^{-3}	830	5.138×10^{-3}	1140	1.934×10^{-2}	1450	7.500×10^{-2}
530	3.487×10^{-3}	840	5.314×10^{-3}	1150	2.089×10^{-2}		
540	3.442×10^{-3}	850	5.503×10^{-3}	1160	2.377×10^{-2}		
550	3.561×10^{-3}	860	5.705×10^{-3}	1170	2.919×10^{-2}		

[1] W. C. Dash and R. Newman, "Intrinsic optical absorption in single-crystal Germanium and Silicon at 77°K and 300°K," Phys. Rev. **99**, 1151–1155 (1955).
[2] G. G. Macfarlane and V. Roberts, "Infrared absorption of Silicon near the lattice edge," Phys. Rev. **98**(6), 1865 (1955).
[3] C. D. Salzberg and J. J. Villa, "Infrared refractive indexes of Silicon, Germanium and modified Selenium glass," J. Opt. Soc. Am. **47**(3), 244–246 (1957).
[4] W. Spitzer and H. Y. Fan, "Infrared absorption in n-type silicon," Phys. Rev. **108**(2), 268–271 (1957).
[5] G. G. Macfarlane, T. P. McLean, J. E. Quarrington, and V. Roberts, "Fine structure in the absorption-edge spectrum of si," Phys. Rev. **111**, 1245–1254 (Sep 1958).
[6] G. G. Macfarlane, T. P. McLean, J. E. Quarrington, and V. Roberts, "Exciton and phonon effect in the absorption spectra of Germanium and Silicon," J. Phys. Chem. Solids **8**, 388–392 (1959).
[7] H. R. Phillip and E. A. Taft, "Optical constants of Silicon in the region 1 to 10 eV," Phys. Rev. **120**(1), 37–38 (1960).
[8] A. A. Vol'fson and V. K. Subashiev, "Fundamental absorption edge of silicon heavily doped with donor or acceptor impurities," Sov. Phys. Semicond. **1**(3), 327–332 (1967).
[9] C. Anagnostopoulos and G. Sadasiv, "Fine structure in the optical-absorption edge of silicon," Phys. Rev. **7**(2), 733–739 (1973).
[10] R. Hulthén, "Optical constants of epitaxial silicon in the region 1-3.3 eV," Phys. Scr. **12**(6), 342–344 (1975).
[11] D. K. Schroder, R. N. Thomas, and J. C. Swartz, "Free carrier absorption in silicon," IEEE J. Solid-St. Circ. **13**(1), 180–187 (1978).
[12] K. G. Svantesson and N. G. Nilsson, "Determination of the temperature dependence of the free carrier and interband absorption in silicon at 1,06 μm," J. Phys. C: Solid State Phys. **12**, 3837–3842 (1979).
[13] H. A. Weakliem and D. Redfield, "Temperature dependence of the optical properties of silicon," J. Appl. Phys. **50**(3), 1491–1493 (1979).
[14] P. E. Schmidt, "Optical absorption in heavily doped silicon," Phys. Rev. B **23**(10), 5531–5536 (1981).
[15] G. E. Jellison and F. A. Modine, "Optical functions of silicon between 1.7 and 4.7 eV at elevated temperatures," Phys. Rev. B **27**, 7466–7472 (1983).
[16] D. E. Aspnes and A. A. Studna, "Dielectric functions and optical parameters of Si, Ge, GaP, GaAs, GaSb, InP, InAs, and InSb from 1.5 to 6.0 eV," Phys. Rev. B **27**(2), 985–1009 (1983).
[17] Edward S. Nartowitz and Alvin M. Goodman, "Evaluation of silicon optical absorption data for use in minority-carrier-diffusion-length measurements by the spv method," J. Electrochem. Soc. **132**(12), 2992–2997 (1985).
[18] J. Geist, A. Migdall, and H. P. Baltes, "Analytic representation of the silicon absorption coefficient in the indirect transition region," Applied Optics **27**(18), 3777–3779 (1988).
[19] G. E. Jellison, "Optical functions of silicon determined by two-channel polarization modulation ellipsometry," Optical Materials **1**, 41–47 (1991).
[20] A. Oschlies, R. W. Godby, and R. J. Needs, "First-principles self-energy calculations of carrier-induced band-gap narrowing in silicon," Phys. Rev. B **45**(23), 13741–13744 (1992).
[21] J. M. Essick and R. T. Mather, "Characterization of a bulk semiconductor's band gap via a near-absorption edge optical transmission experiment," Am. J. Phys. **61**(7), 646–649 (1993).
[22] E. Daub, "Photolumineszenz von Silizium," PhD thesis, University of Karlsruhe, Germany, 1995.
[23] E. Daub and P. Würfel, "Ultralow values of the absorption coefficient of Si obtained from luminescence," Phys. Rev. Letters **74**(6), 1020–1023 (1995).
[24] M. A. Green and M. J. Keevers, "Optical properties of intrinsic silicon at 300 K," Prog. Photovolt: Res. Appl. **3**, 189–192 (1995).
[25] M.J. Keevers and M.A. Green, "Absorption edge of silicon from solar cell spectral response measurements," Appl. Phys. Lett. **66**(2), 174–176 (1995).
[26] M. J. Keevers and M. A. Green, "Extended infrared response of silicon solar cells and the impurity photovoltaic effect," Sol. Energ. Mat. Sol. C. **41**(42), 195–204 (1996).
[27] A. Neisser and M.A. Green, "Very low absorption coefficients of silicon at low temperatures from spectral response measurements," in *Proc. 2nd WPVSC*, *Vienna, Austria* (1998) pp. 136–139.
[28] A. Neisser, "Spectral response measurements on silicon solar cells in the range of 1 ev to 5 ev photon energy at different temperatures," Master's thesis, Technische Universität Berlin, Germany, 1998.
[29] J. Geist, *Handbook Of Optical Constants Of Solids III* (Academic Press, 1998).

[30] C. M. Herzinger, B. Johs, W. A. McGahan, J. A. Woollam, and W. Paulson, "Ellipsometric determination of optical constants for silicon and thermally grown silicon dioxide via a multi-sample, multi-wavelength, multi-angle investigation," J. Appl. Phys. **83**(6), 3323–3336 (1998).
[31] T. Trupke, E. Daub, and P. Würfel, "Absorptivity of silicon solar cells obtained from luminescence," Sol. Energ. Mat. Sol. C. **53**, 103–114 (1998).
[32] M.A. Green, "Self-consistent optical parameters of intrinsic silicon at 300 K including temperature coefficients," Sol. Energ. Mat. Sol. C. **92**, 1305–1310 (2008).
[33] T. R. Harris, "Optical Properties Of Si, Ge, GaAs, GaSb, InAs, And InP at Elevated Temperatures," PhD thesis, Air Force Institute Of Technology, Ohio, USA, 2010.
[34] C. Schinke, K. Bothe, P. C. Peest, J. Schmidt, and R. Brendel, "Uncertainty of the coefficient of band-to-band absorption of crystalline silicon at near-infrared wavelengths," Appl. Phys. Lett. **104**(081915), (2014).
[35] H. T. Nguyen, F. E. Rougieux, B. Mitchell, and D. Macdonald, "Temperature dependence of the band-band absorption coefficient in crystalline silicon from photoluminescence," J. Appl. Phys. **115**, 043710 (2014).
[36] S. C. Baker-Finch, K. R. McIntosh, D. Yan, K. C. Fong, and T. C. Kho, "Near-infrared free carrier absorption in heavily doped silicon," J. Appl. Phys. **116**(063106), (2014).
[37] Joint Committee for Guides in Metrology, *Guide to the expression of uncertainty in measurement* (BIPM, Paris, 2008).
[38] H. G. Tompkins, *Handbook of Ellipsometry* (William Andrew, Inc, 2005).
[39] I. N. Bronstein and K. A. Semendjaev, *Taschenbuch der Mathematik* (Verlag Harri Deutsch, 2001).
[40] P. Würfel, T. Trupke, and T. Puzzer, "Diffusion lenghts of silicon solar cells from luminescence images," J. Appl. Phys. **101** (2007).
[41] D. Hinken, K. Bothe, K. Ramspeck, S. Herlufsen, and R. Brendel, "Determination of the effective diffusion length of silicon solar cells from photoluminescence," J. Appl. Phys. **105**(10), 104516 (2009).
[42] C. Schinke, D. Hinken, J. Schmidt, K. Bothe, and R. Brendel, "Modeling the spectral luminescence emission of silicon solar cells and wafers," IEEE J. Photovolt. **3**(3), 1038–1052 (2013).
[43] P. Würfel, "Generalized planck's radiation law for luminescence via indirect transitions," Appl. Phys. A **60**, 67–70 (1995).
[44] U. Rau, "Reciprocity relation between photovoltaic quantum efficiency and electroluminescent emission of solar cells," Phys. Rev. B **76** (2007).
[45] Joint Committee for Guides in Metrology, *International vocabulary of metrology - Basic and general concepts and associated terms (VIM)* (BIPM, Paris, 2008).
[46] W. Wöger, "Remarks on the en-criterion used in measurement comparisons," PTB-Mitteilungen **109**, 24–27 (1999).
[47] J. A. Woollam Co, *Guide to using WVASE32* (J. A. Woollam Co., Inc, 2010).
[48] J.H. Mazur, R. Gronsky, and J. Washburn, "High resolution electron microscopy studies of native oxide on silicon," in *Proc. 3rd Oxford Conferenceon Microscopy of Semiconducting Materials*, (1983) pp. 77–82.
[49] G. E. Jellison, Jr., and F. A. Modine, "Parameterization of the optical functions of amorphous materials in the interband region," Appl. Phys. Lett. **69**(3), 371–373 (1996).
[50] J. Tauc, R. Grigorovici, and A. Vancu, "Optical properties and electronic structure of amorphous germanium," Phys. Stat. Sol. **15**, 627–637 (1966).
[51] P. C. Peest, C. Schinke, K. Bothe, and R. Brendel, to be published.
[52] C. Schinke, "Uncertainty of the Coefficient of Band-to-Band Absorption of Crystalline Silicon," PhD thesis, Leibniz University of Hanover, Germany, 2015, to be submitted.
[53] S. Winter, T. Wittchen, and J. Metzdorf, "Primary reference cell calibration at the PTB based on an improved DSR facility," in *Proc. 16th EUPVSEC*, *Glasgow, Great Britain* (2000) pp. 2198–2201.
[54] S. Winter, "Analyse und Verbesserung der rückführbaren Kalibrierung von Solarzellen," PhD thesis, Technische Universität Carolo-Wilhelmina, Braunschweig, Germany, 2004.
[55] M. Schmelling, "Averaging measurements with hidden correlations and asymmetric errors," Technical Report 1 (Max-Planck Institute for Nuclear Physics, Heidelberg, Germany, 2000).
[56] M.A. Green, *Silicon Solar Cells - Advanced Priciples and Practice* (University of New South Wales, 1995).
[57] R. Brendel, M. Hirsch, R. Plieninger, and J.H. Werner, "Quantum efficiency analysis of thin-layer silicon solar cells with back surface fields and optical confinement," IEEE T. Electron Dev. **43**, 1104–1113 (1996), doi:10.1109/16.502422.
[58] See supplemental material at http://dx.doi.org/10.1063/1.4923379 for tabulated data of the absorption coefficient as determined in this work.
[59] B. Mitchell, M.K. Juhl, M.A. Green, and T. Trupke, "Full spectrum photoluminescence lifetime analyses on silicon bricks," IEEE J. Photovolt. **3**(3), 962–969 (2013) ISSN 2156-3381.
[60] C. Schinke, P. C. Peest, J. Schmidt, R. Brendel, K. Bothe, M. R. Vogt, I. Kröger, S. Winter, A. Schirmacher, S. Lim, H. Nguyen, and D. MacDonald, "Experimental determination of the uncertainty of the absorption coefficient of crystalline silicon," in *Proc. 5th SiliconPV*, *Konstance, Germany* (2015) Accepted.